Environmental Earth Sciences (2025) 84:338
https://doi.org/10.1007/s12665-025-12196-2

ORIGINAL ARTICLE

Monitoring and simulation of bridge pier scour and deposition processes in flood events

Fong-Zuo Lee[1] · Jihn-Sung Lai[2] · Yung-Bin Lin[3] · Kuo-Chun Chang[4]

Received: 25 August 2024 / Accepted: 8 March 2025

Abstract
Bridge failure caused by flood-induced scour around piers remains the primary threat to traffic disruption and life losses. Real-time monitoring of scour variations is crucial to avoid bridge failure. The scour monitoring system is developed and implemented in the field, consisting of vibration-based MEMS (micro-electromechanical systems) arrayed sensors for water level and flow velocity measurement. The scour monitoring system records scour and deposition depth changing over time at the bridge pier in flood events. A numerical simulation module combining one-dimensional and two-dimensional mobile-bed hydrodynamic models is established to calculate scour and deposition depths based on field hydrological conditions. The field-measured data from the real-time scour monitoring system are employed for model validation. Due to the complexity of hydraulic sediment transport mechanisms around the pier, several local scour formulas have been evaluated to verify their applicability. Using field-measured scour depth data, a suitable local scour formula for the Mingchu Bridge in the Cho-Shui River is developed. The real-time scour monitoring system coping with the numerical simulation module developed in this study can provide accurate information on scour and deposition processes at the bridge pier, which is helpful for decision-makers to assess the risk of bridge damage and the timing of bridge closure. Finally, the proposed bridge safety curve referring to four bridge warning stages based on the pier foundation characteristics, as a determinate relationship between scoured bed level and discharge, has been established to assist bridge managers in making rational decisions on bridge closures during floods.

Keywords Bridge failure · Scour monitoring · Hydrodynamic model · Scour · Deposition

✉ Yung-Bin Lin
yblin@ncree.narl.org.tw

Fong-Zuo Lee
fzlee@nchu.edu.tw

Jihn-Sung Lai
jslai525@ntu.edu.tw

Kuo-Chun Chang
ciekuo@ntu.edu.tw

1 Department of Civil Engineering, National Chung Hsing University, 145 Xingda Rd., South Dist., Taichung City 402202, Taiwan, ROC

2 Hydrotech Research Institute, National Taiwan University, No. 1, Sec. 4, Roosevelt Rd., Taipei City 106319, Taiwan, ROC

3 National Center for Research on Earthquake Engineering, No. 200, Section 3, Xinhai Rd., Da'an Dist., Taipei City 106219, Taiwan, ROC

4 Department of Civil Engineering, National Taiwan University, No. 1, Sec. 4, Roosevelt Rd., Taipei City 106319, Taiwan, ROC

Introduction

Hydraulics-related scour of pier foundations is the primary cause of bridge failure, especially during flood events. Scour occurs when the bed materials around the pier are eroded, leaving the bridge piers and abutments in an unsafe condition or even in danger of collapse (Prendergast and Gavin 2014; Wang et al. 2017; Bento et al. 2020). The causes of bridge collapse or failure can be strongly related to hydrological and hydraulic conditions, such as scouring at the bridge foundation. Therefore, evaluating the extreme hydrological events of various return-period floods is critical to qualitatively assess the bridge scour risk by associating its scour depth with foundation depth (Proske 2018; Bento et al. 2020, 2024). In many East Asian countries, such as Taiwan and Japan, severe bridge failure problems arise due to frequent typhoon flood events. During flood seasons, typhoons or heavy storm rainfall bring high flow discharge and sediment, causing significant scour problems and threatening the integrity of pier structures. Scour failure tends to occur suddenly and without prior warning to the structures. In Taiwan, many bridge failure cases occurred during Typhoons Herb (1996), Bilis (2000), Sinlaku (2008), and Morakot (2009) (Lu et al. 2008; Lin et al. 2010; Hong et al. 2016). In Typhoon Morakot, the most catastrophic disaster, 675 deaths were reported, along with substantial economic losses; meanwhile, typhoon-induced floods damaged 193 bridges.

Research has focused on developing scour monitoring schemes and devices to better understand the evolution of scouring and deposition processes around bridge foundations. The performance of the scour monitoring system depends on how accurately it can measure the evolution of scour depth at a bridge pier. However, the flow mechanism of scouring around the bridge pier is complex, and characterizing the flow velocity field and geometry surrounding the scour hole is usually obtained by conducting flume experiments, which has been investigated by various researchers (Lin et al. 2005; Deng and Cai 2010; Wang et al. 2017; Bento et al. 2018, 2021). Maximum scour may occur near the peak of flood discharge, at which point the scour hole may tend to refill as the floodwaters recede. However, these scour holes may not be detected in time before they are refilled as the flood subsides. Various depth-measuring instruments have been developed to monitor changes in riverbed levels and the formation of scour holes around bridge piers. Prendergast and Gavin (2014) reviewed bridge scour monitoring techniques and noted that using discrete-depth recording instrumentation outperforms conventional visual inspection methods. According to the literature, field-installed devices for scour monitoring or measurement include acoustic emission (AE) sensors (Invernizzi et al. 2011), vibration-based methods (Fisher et al. 2013a, b; Zheng et al., 2015; Bao et al. 2017; Wang et al. 2018), fiber optic sensors (Ballio et al., 2003; Lin et al. 2005, 2006; Zhou et al. 2011; Zarafshan et al. 2012; Ye et al. 2018; Kong et al. 2017), MEMS sensors (Lin et al. 2010), the sonic echo approach (Rashidyan et al. 2017), time-domain reflectometry (TDR) (Yu et al. 2013; Gao and Yu 2015; Lin et al. 2017; Miyata and Fujita 2018), piezoelectric sensors (Wang et al. 2012; Ding et al. 2016), strain sensors (Wu et al. 2018), and bridge/pier natural frequency variation (Ahmed and Rajaratnam 1998; Melville et al. 2006; Parker 1990; Chiew 2004; Chang et al. 2013; Federico et al. 2003). A vibration-based sensor for scour measurement developed recently shows potential for operational advantages (Lin et al. 2021).

A device for monitoring bridge scour with a data acquisition system faces challenges in surviving flood events, such as extreme flood flows with massive debris impact, which could result in bridge failure. Moreover, the vibration-based sensors used in the field must provide long-term waterproofing performance as they are buried in the riverbed. As reported in the literature, field data is limited due to the observational difficulties during floods (Wang et al. 2017; Lin et al. 2021). These empirical scour formulas may not be accurate enough for field applications without sufficient field-measured data as inputs. Therefore, it is necessary to develop a field-based real-time monitoring system to observe and track the evolution of scour depth at the bridge pier.

However, these scour monitoring techniques have been limited to specific applications. They include the intense demand for routine maintenance, low resistance to environmental factors (e.g., extreme floods, large woody debris, and high turbidity), and high susceptibility to noise caused by sediment particles in the flow. Additionally, some of these devices cannot detect the maximum scour depth or the refilling of scour holes. The scour monitoring system would be exposed to harsh environmental conditions for long-term monitoring. Therefore, the characteristics of a reliable, real-time monitoring system should include high durability and sensitivity to withstand such catastrophic conditions leading to bridge failure. Monitoring real-time variations in scour and deposition helps engineers design safer and more cost-effective bridges.

Bridge scour generally occurs in the forms of general scour, contraction scour, and local scour, all of which are associated with the flow field evolution and the progression of scouring and refilling around the pier foundation. General scour occurs naturally in river channels, involving the aggradation and degradation of the riverbed. Contraction scour occurs due to the reduction in the cross-sectional area of the river, which increases flow velocity and bed shear stresses, often due to the construction of bridge piers and abutments (Arneson and Abt 1998). Finally, local scour occurs when horseshoe vortices, along with downflow, form in the immediate vicinity of the pier, creating localized erosion around the pier (Melville and Coleman 2000). Among these three types of scour, local scour is usually the leading cause of most bridge damage (Lu et al. 2008; Hong et al. 2016). The relevant hydraulic parameters for local scour include the diameter of the bridge pier, approaching flow depth and velocity, sediment transport capacity, and grain size. Therefore, measuring or simulating flow depth, velocity, and sediment transport capacity are the main tasks in the field. Many empirical formulas for local scour depth estimation have been established and are used for practical design. However, real-time scour and deposition depth monitoring at bridge piers in situ is challenging, especially during floods. Additionally, estimating local scour depth during the refilling process remains a significant challenge in field measurements, especially during the recession limb of a flood hydrograph (Link et al. 2020). Most studies focus on the temporal evolution of local scour in laboratory settings without implementing field data (Yang et al. 2020). Furthermore, most studies concentrate on scour prevention using flume data and specific external structures or geometries in the laboratory (Gupta et al. 2023; Vahdati et al. 2024). Therefore, the primary aim of this study is to apply a reliable simulation model with feasible scour formulas and real-time, in situ scour monitoring data to understand better bridge pier scour and deposition processes during flood events.

Although numerous studies on bridge scour have been reported in the literature, numerical simulations of scour-depth variations with in situ measurements during floods are limited. Proper prediction of temporal scour-depth changes using numerical hydrodynamic models can provide valuable early warning information for bridge failure. Predicting riverbed changes is essential for recognizing any potential aggravation or degradation of the riverbed level, particularly around bridge piers. In flood events, sediment transport can simulate the flow field and pattern through a numerical hydrodynamic model to assess the time variation of the total scour depth at the pier. The Sedimentation and River Hydraulics Two-Dimensional (SRH-2D) model is a depth-averaged 2D hydraulic and sediment model designed for simulating flows in fluvial rivers with hydraulic structures such as bridge piers (Lai 2020). The model is suitable for modeling riverbed migration, including the general scour of the riverbed. However, the numerical hydrodynamic model cannot directly compute the local scour depth. Using commonly employed empirical formulas, the local scour depth is calculated from the simulated water level and velocity results of the SRH-2D model.

For practical engineering purposes, the total scour depth is the sum of the general scour from the numerical hydrodynamic model and the local scour calculated using empirical formulas. The predictive information on scour-depth variations can provide valuable data for early warning of bridge failure. Moreover, based on the scour-depth elevation and the bridge pier foundation, it is essential to provide an assessment of scour risk qualitatively under various hydrological and hydraulic conditions, which will assist the bridge managers in making appropriate decisions on bridge operations (Clopper et al. 2014; Bento et al. 2022).

This study has developed a reliable and durable scour monitoring system designed for real-time and long-term monitoring. The performance and feasibility of the system have been evaluated through scour-depth monitoring results from two typhoon-induced flood events. Additionally, a hydrodynamic model combining one-dimensional and two-dimensional hydraulic models with sediment transport has been developed and validated using the measured scour data. A suitable local scour formula was also developed, regressed from field-measured scour data. The hydrodynamic model can be implemented to predict the scour depth of piers before a flood occurs. Then, for the assessment of scour risk, the bridge safety curve based on the relationship between scoured bed level and discharge is established to assist bridge managers in deciding the timing of bridge closures.

Materials and methods

Site description and hydrological data

The Mingchu Bridge spans the Cho-Shui River, connecting two major areas: Mingjian Township (to the north) and Zhushan Township (to the south), as shown in Fig. 1(a). Located in central Taiwan, the bridge is situated 56 km upstream from the estuary of the Cho-Shui River, which flows westward into the Taiwan Strait. As a key transportation route, the Mingchu Bridge, constructed in 1990, is located 6.5 km downstream of the Chi-Chi Weir. Significant riverbed erosion, scour of the pier foundations, and damage to the river embankment have frequently occurred during typhoon floods or heavy rainfall events (Guo et al. 2017; Lee et al. 2018a, b). The riverbed between Chi-Chi Weir and the Mingchu Bridge has experienced erosion due to the steep slope and limited sediment supply. Most of the coarse sediments are trapped in the upstream river reach of the Chi-Chi Weir. After the Chi-Chi earthquake in 1999, the bridge was damaged and rebuilt in 2000. The new Mingchu Bridge is 720 m long and comprises 13 concrete beam spans supported by cylindrical piers (2.38 m in diameter).

The natural drainage area of the Cho-Shui River watershed is approximately 2300 square kilometers, and the bed slope of the river around the bridge is about 0.7%. The peak discharge for the 100-year return-period flood, which serves as the design flood for levee protection, is estimated to be 20,500 m^3/s, based on frequency analysis provided by the Water Resources Agency, Taiwan. The mean annual discharge of the Cho-Shui River is approximately 139 m^3/s. The mainstream, with a width of 300 m at the northern end (right bank), flows underneath the Mingchu Bridge between Pier P1 and Pier P7, as illustrated in Fig. 1(b). The bridge piers are supported on pile caps with concrete piles extending below the underside of the cap.

The simulation domain for the one-dimensional (1D) hydrodynamic modeling is selected along the river reach, from the upstream inflow boundary at the Chi-Chi Weir to the downstream boundary at the estuary, as shown in Figs. 1(a) and 1(d). The 1D simulation domain includes two tributaries that flow into the main river, and the hydrographs of inflow discharges from these tributaries are provided by field measurement data at Yanping and Longmen Bridges, as illustrated in Fig. 1(a). The two-dimensional (2D) simulation domain for the numerical hydrodynamic modeling is located between two surveyed cross-sections, with the upstream inflow boundary 1200 m upstream of

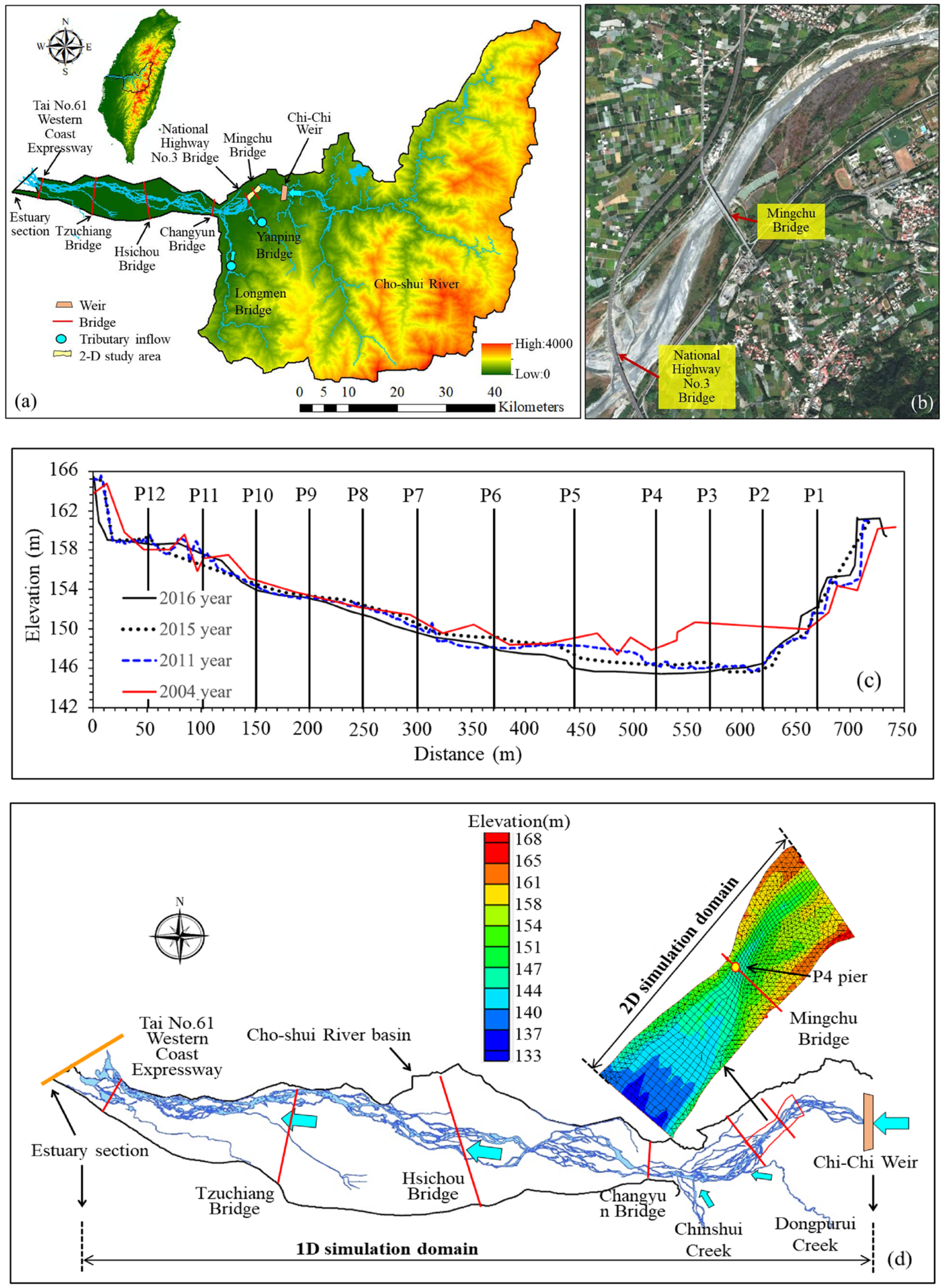

Fig. 1 The study site at Mingchu Bridge: **a** location and watershed maps of the Cho-Shui River Basin; **b** aerial image; **c** bed elevation variations at the bridge viewing from upstream; **d** numerical simulation domain

the Mingchu Bridge and the downstream boundary at the National Highway No. 3 Bridge, as shown in Fig. 1(a). The bed elevations within the simulation domain range from EL 135.4 m to EL 167.8 m above sea level. The median grain size (d_{50}) of the bed material around the Mingchu Bridge was 1.52 mm, with a geometric standard deviation of sediment size of 7.45 in 2014 (Hong et al. 2016). This study investigates typhoon flood events from 2015 and 2016 in relation to bridge scour. Additionally, flood discharge scenarios with return periods of $Q_{1.1}$, Q_2, Q_{10}, and Q_{100} are implemented to assess the effects of scour depth variations at the river cross-section of the Mingchu Bridge. The Chi-Chi Weir provides the upstream inflow discharge for the 1D model, and the downstream boundary at the estuary provides the water level hydrograph. The hydrographs of peak flood discharges ranged from 2000 m^3/s to 20,500 m^3/s, with the water level ranging from EL 147.11 m to EL 155.51 m at the Mingchu Bridge. Based on the bathymetry survey and the literature reference of Hong et al. (2016), the main channel and flow area are close to Pier 4. Therefore, the monitoring data of scour depth evolution at Pier P4 is adopted for numerical modeling verification. The main objective of the present study is to evaluate the applicability of scour depth simulation for developing an early warning at the Mingchu Bridge.

The scour monitoring system was installed on bridge Pier P4, as shown in Fig. 1(c). This system is designed to measure variations in bridge scour depth using ten vibration-based MEMS arrayed sensors. These sensors were tested in the laboratory for durability and reliability before being deployed in the field. This paper used the vibrating signal of a MEMS accelerometer. Initially, the MEMS accelerometers are packaged in waterproof stainless-steel balls and embedded into the riverbed, a design that has been proven to withstand harsh flood environments for long-term operational use, as mentioned. These MEMS sensors are arranged vertically in an array, safely installed in a calculated steel cage, and embedded into the riverbed. The sensor will be exposed to turbulent flow when it encounters rush water in flood to wash away the riverbed soil. The turbulent energy will induce vibration signals from the MEMS accelerometer. As the flood recedes, the riverbed will return to its deposit state, and the MEMS accelerometer will be buried in the soil again. At this time, the vibration signal of the MEMS accelerometer gradually becomes stable and is no longer affected by the impact of the vibration signal analysis. The sediment deposition depth is then obtained. The wireless station includes a wireless sensor network (WSN) system and a CCTV camera with a night infrared light source, focusing on the water flow around the pier. Therefore, the system design is robust and efficient enough to endure debris impact, sustain long-term service, and survive flood events.

Prediction of bridge pier scour depth and field scour depth monitoring were conducted at the Mingchu Bridge site, located in the middle of the Cho-Shui River, the longest river in Taiwan, as shown in Fig. 1(a). Because the scour monitoring system developed herein needs to be embedded into the river bed, the drilled machine will be used according to the safe depth of the bridge pier foundation. This part of the drilling construction requires more funds if large gravel and rock are distributed around the riverbed. Exceptionally, when the monitoring target pier is located in a deep groove area with water all year round, civil construction on this section of scour monitoring installation will be more expensive. Therefore, this paper aims to accumulate more actual scour measurement data to establish scour depth and bridge pier safety prediction models for developing a reliable river-basin disaster monitoring and bridge-scour early-warning system in this study.

The watershed above the Mingchu Bridge is approximately 2105 km^2. The Chi-Chi Weir is located about 6.5 km upstream of the Mingchu Bridge and serves as the upstream boundary for this study. Because no tributary flows occur between the weir and the bridge, the flow discharge measured at the Chi-Chi Weir is nearly identical to the flow at the bridge. However, the downstream river reach includes two tributaries, and therefore, the tributary discharge is derived from field measurement data at Yanping and Longmen bridges. The downstream boundary condition for the water level is set at the Tai No. 61 Western Coast Expressway. The median grain size of bed material around the Mingchu Bridge, d_{50}, was approximately 62 mm, indicating a highly non-uniform gradation. The Mingchu Bridge is situated in the flood channel, consisting of 13 spans and 12 cylindrical columns (2.8 m in diameter). Each column rests on a piled foundation (12 m cap width), buried below the stream bed (Hong et al. 2014).

In addition, the monitoring system should possess high durability and sensitivity. To take the necessary precautions against such catastrophic conditions, a monitoring system that can reliably detect scour formation without adversely affecting environmental conditions is essential (Fisher et al. 2013a, b). Since 2016, disaster monitoring technology applications and early warning simulations in the Cho-Shui River basin have been investigated. The bridge pier monitoring sensor and numerical model are implemented to study bridge pier scour depth prediction. As a result, in this study, the development principle is based on a MEMS vibration sensor, which vibrates at significantly higher amplitudes due to the turbulent flow surrounding the bridge piers, both up and down the riverbed. The sensor setup is located at Pier P4 of the Mingchu Bridge, with the setup depth ranging from the riverbed to the elevation level of 143 m. The deepest monitoring depth is constrained at elevation 143 m (as shown in Fig. 1(c)).

Scour monitoring system

Laboratory fabrication

Vibration measurements by the vibration-based MEMS sensors provide a great promise of accurate monitoring to detect any deviation from normal conditions. Using the MEMS accelerometer is a simple and suitable technology for sensing. The application of MEMS accelerometers has been widely investigated and utilized to detect linear acceleration. Similar to many available accelerometers on the market today, the vibration-based sensor LSM303DLH from STMicroelectronics is used as a scour positioning indicator in this study. This sensor is a digital 3-axis accelerometer packaged inside a plastic case, sealed with liquid silicone compound glue to create a waterproof layer, as shown in Fig. 2(a). The sensor node is then housed in a stainless steel ball with an RS-485 signal line and further waterproofed with a full-fill resin, as shown in Fig. 2(b). In Figs. 2(c, d), these scour-arrayed sensors, assembled in a rebar cage, are used to measure the vibration signals as they emerge from the riverbed and vibrate due to the

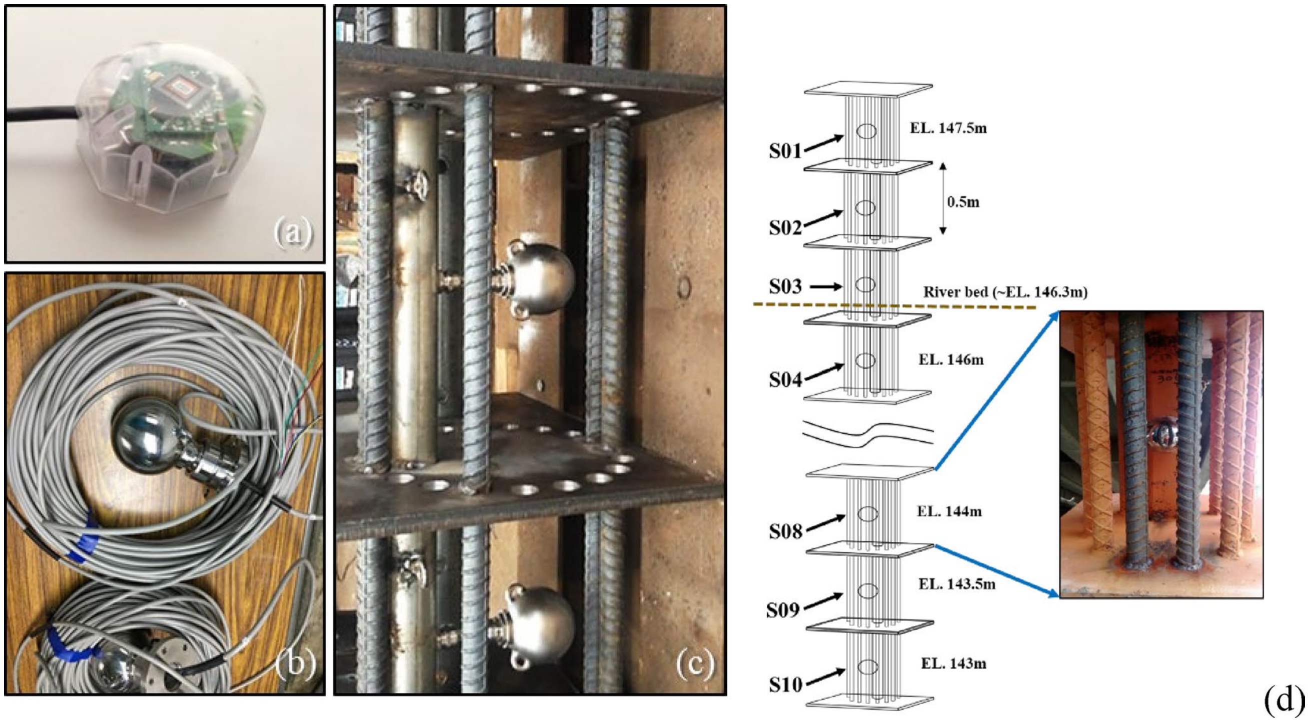

Fig. 2 The scour monitoring system assembled in the lab **a** a packaged node with a MEMS sensor; **b** each sensor node sealed by a steel ball with RS-485 signal line; **c** protected by the steel rebar cage; **d** arrayed sensor nodes (S01 ~ S10) installed on Mingchu Bridge at pier P4

flowing floodwater. The experimental tests were conducted in the laboratory flume at the Hydrotech Research Institute of National Taiwan University, Taipei, Taiwan, to validate these scour sensing devices by capturing responses to bed-level variations.

Each sensor node serves as a scour positioning indicator. In the scour monitoring system, the distance between each sensor node is 0.5 m. If a sensor node is buried in the bed, no reading is produced, and the sensor remains stationary until floodwater flow removes the surrounding sediments. Once the sensor node is exposed to the floodwater, it vibrates in response to the time-varying flow turbulence, and a scour hole is formed during this process. Subsequently, when sediment deposition occurs and fills the scour hole, the sensor stops vibrating and resumes a stationary state. Therefore, detecting changes in the vibration responses of individual sensor nodes in the sensor array allows for assessing riverbed changes during the scour and sedimentation processes. Before being deployed in the field, these packaged sensor nodes for bridge scour measurement were tested under different flow velocities in the laboratory to ensure their performance, particularly their long-term waterproof characteristics. Proper packaging to resist harsh environments, such as fast-flowing floodwater and debris impacts, is a crucial robustness factor for bridge pier scour measurements.

Field installation

The scour monitoring system with arrayed MEMS sensors was designed and fabricated to meet waterproof requirements and resist the adverse impact forces of drifting debris and moving sediments. The system comprises ten sensor nodes, fabricated and aligned with even spacing to form a sensor array, which is then fastened inside a steel rebar cage for additional protection, as shown in Fig. 3(a). The underwater performance of each sensor node for field durability was tested before on-site installation to ensure survival in a flooding environment. The schematic layout for field deployment is presented in Fig. 3(b). The array of ten sensor nodes, housed in the protected steel rebar cage, was mounted on pier P4 at the top of the pile cap. The wireless station contains the WSN systems with a data logger and a CCTV camera with a night infrared light source, focusing on the water flow around the pier. The system is designed to automatically record the vibration responses of the sensor nodes and transmit the recorded data to a cloud processor for scour analysis.

Additionally, scour processes are highly correlated with flow velocity and water level. Therefore, measuring real-time flow velocity and water level is critical in the field study. Installed at the outer edge of the bridge deck, as shown in Fig. 3(a), the Mingchu gauging station consists of a radar

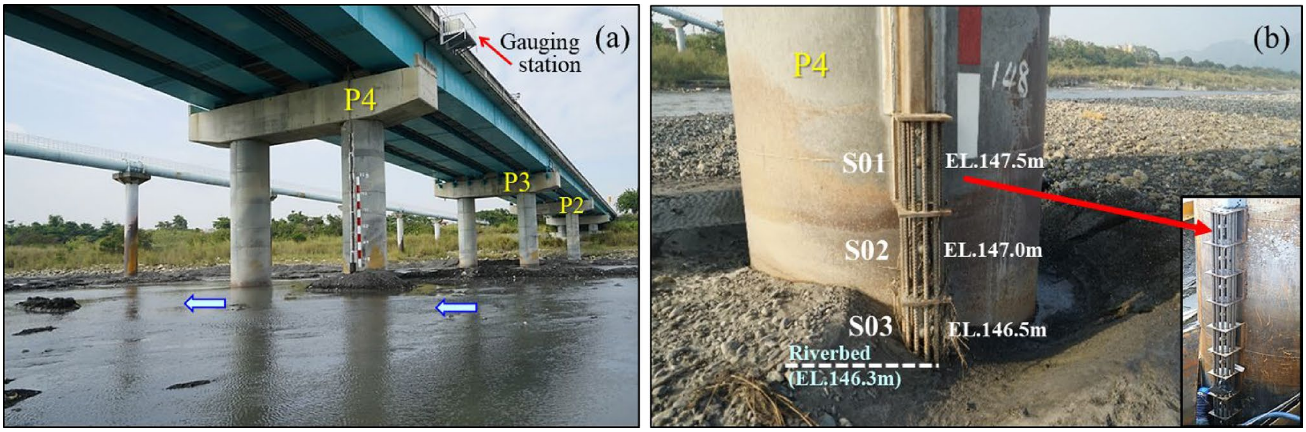

Fig. 3 Field deployment of the scour monitoring system **a** viewing P4 of Mingchu Bridge from upstream; **b** installation on the pier and in situ inspection after Typhoon Megi flood

water-level meter and a radar velocimeter located near Pier P4 to provide the field-measured data. The details of how the velocity measurements were conducted can be found in the Highway Bureau (2020). A radar velocimeter was used to measure the water surface velocity. The depth-averaged velocity, which is half the value of the water surface velocity, is also discussed in the Highway Bureau (2020). The station records real-time water level and flow velocity for hydrodynamic model calibration and scour depth estimation. As illustrated in Fig. 3(b), the ten scour sensor nodes, denoted as S01–S10, were installed in descending order of elevation, with a spatial interval of 0.5 m between each sensor. However, not all the sensor nodes were installed below the riverbed level in this study. Specifically, S01, S02, and S03 were positioned above the original riverbed level, which had an elevation of approximately EL.146.3 m above sea level, coinciding with the depth below S03. Due to the unique site terrain and hydrological conditions of the Cho-Shui River, the riverbed around the Mingchu Bridge typically remains dry during Taiwan's dry season (from October to February), causing sensors S01, S02, and S03 to be exposed to air.

Method for modeling scour-depth evolution

Hydrodynamic mobile-bed simulation

As described in the literature, field-measured scour data is limited due to observational challenges during floods (Wang et al. 2017; Lin et al. 2021). Although previous research has focused on numerical simulations of bridge scour depth, predicting scour-depth variations using field-measured data for model validation during floods remains limited. Hydrodynamic mobile-bed modeling allows for the accurate forecasting of temporal scour-depth changes, providing crucial early warning information for bridge failure.

A fluvial river with a mobile riverbed is a complex dynamic system governed by mathematical equations describing water–sediment interactions. Sediment transport in a mobile riverbed can be coupled with the flow field and pattern through a numerical hydrodynamic model to assess the time variation of total scour depth at the bridge pier. In the present study, hydrodynamic mobile-bed modeling is performed by combining one-dimensional (1D) and two-dimensional (2D) hydraulic models with sediment transport and validating the results using field-measured scour data.

As illustrated in Fig. 1(d), the 1D simulation domain for the hydrodynamic modeling extends from the upstream inflow boundary at the Chi-Chi Weir to the downstream boundary at the estuary. This 1D simulation domain includes two tributaries, Chinshui Creek and Dongpurui Creek, with discharge hydrographs imposed as inflow boundaries at Yanping and Longmen Bridges. The 2D simulation domain for the hydrodynamic modeling is located between two surveyed cross-sections: the inflow boundary 1200 m upstream of the Mingchu Bridge and the downstream boundary at the National Highway No. 3 Bridge. The simulated outputs (i.e., water depth, velocity, and sediment discharge hydrographs) from the 1D model serve as boundary inputs for the 2D model.

For 1D hydrodynamic mobile-bed modeling, the SRH-1D (Sedimentation and River Hydraulics – One Dimension) model is adopted to simulate unsteady flows with sediment transport in natural rivers (Greimann 2011). The SRH-1D model is specifically developed for studying open-channel flows with sediment transport and can simulate subcritical and supercritical flow, as well as steady and unsteady flows, in river morphology generated by riverbed aggregation or degradation. When considering hydraulic scour depths, most open-channel flows are assumed to involve shallow water. Therefore, the effect of vertical flow motions is not calculated if downflow along the bridge pier is considered in local scour formulas. In conjunction with the SRH-1D model, the two-dimensional (SRH-2D) sedimentation and river hydraulics model is employed in this study. The SRH-2D model is a depth-averaged 2D model developed for simulating open-channel flows with mobile-bed conditions in fluvial rivers. The model is based on solving the 2D shallow-water flow equations using the finite-volume numerical method on an unstructured hybrid mesh system (Lai 2010). It can simulate subcritical and supercritical flow, steady and unsteady flow, and dry and wetted flow, which are generated by riverbed topography with hydraulic structures such as embankments and bridge piers (Sakhaee 2020). Moreover, the model has been validated in several experimental or field cases involving shallow-water flows (Lai 2009, 2010, 2017, 2020), demonstrating its suitability for practical applications in hydraulic engineering related to horizontal flow circulation, lateral variations, etc.

The total hydraulic scour depth in front of a pier is affected by general scour, local scour, and contraction scour (Deng and Cai 2010). However, because the spans of the bridge piers are substantially larger than the pier diameters, contraction scour is considered minor in this study. Sediment transport in a water column includes both suspended load and bed load. The elevation of a mobile-bed surface changes due to net erosion and deposition. Elevation changes are contributed by all sediment size classes and are computed based on the net sediment exchanges between those in the water column and those in the active layer. The SRH-2D model is suitable for modeling riverbed migration, such as general scour of the riverbed. However, the numerical hydrodynamic model cannot directly simulate local scour depth (Guo et al. 2014; Hogan 2018). Instead, local scour depth can be calculated using the simulated water level and velocity results from the SRH-2D model in conjunction with appropriate empirical formulas. For practical purposes, the total scour depth is the sum of the general scour predicted by the hydrodynamic model, with local scour calculated using the empirical formulas. The predictive information on total scour depth variations can provide valuable data for early warning of bridge failure. The total scour depth evolution is simulated using the hydrodynamic mobile-bed model, along with selected local scour formulas and the sediment transport equation. This predictive information on total scour depth variations is crucial for early warning of potential bridge failure.

Scour depth estimation

The total scour depth at a pier is affected by general scour and local scour. The general scour has resulted from bed material transportation, which includes suspended load and bed load. The general scour estimation is based on the simulation of bed elevation changes calculated from the SRH-2D model, which is obtained using the bed load equation (Parker 1990) for the bed load combined with an advection–dispersion equation for the suspended load. The Parker's (1990) equation is well suited in the mixed sand-gravel rivers. The transport equation for sediment size class k may be expressed as:

$$\frac{S_g(4\pi(d_k/2)^3/3)/p_o g(s-1)}{(\tau_b/\rho)^{1.5}} = P_{ak}G(\varphi_k),\ \ \phi_k = \frac{\theta_k}{\theta_r}\left(\frac{d_k}{d_{50}}\right)^a \quad (1)$$

$$G = \left\{ \begin{array}{l} 11.933\left(1-0.853/\phi_k\right)^{4.5} \\ .00218\exp\left[14.2\left(\phi_k-1\right)-9.28\left(\phi_k-1\right)^2\right] \\ .00218 \end{array} \right\}, \quad \begin{array}{c} \phi_k > 1.59 \\ 1.0 \le \phi_k \le 1.59 \\ \phi_k \le 1.0 \end{array} \quad (2)$$

In the above, S_g is the general scour per unit width. p_o is the sediment porosity (=0.4). P_{ak} is the volumetric fraction of sediment size class k on the bed surface. $s = \rho_s/\rho - 1$. ρ and ρ_s are the water and sediment density, respectively. g is the gravitational acceleration. τ_b is bed shear stress. $\theta_k = \tau_b/[\rho g(s-1)d_k]$ is Shield's parameter of sediment size class k. θ_r is the reference Shield's parameter. d_k is the diameter of sediment size class k. d_{50} is the median diameter of the sediment size mixture in the bed. Ideally, θ_r and α should be calibrated using available data specific to the stream being simulated. In the absence of site-specific data, guidance can be found in various references, including Bungton and Montgomery (1997), Wilcox and Crowe (2003), Komar (1989), Greimann and Vandeburg (2008), Andrews (2000), WRA (2008), Lee et al. (2018a), Lai (2020), Duffy et al. (2024), and Yang et al. (2024). Generally, θ_r ranges from 0.03 to 0.08, while α varies between 0.11 and 0.91. For this study, based on the same watershed area and the parameter validation of θ_r and α provided by WRA (2008) and Lee et al. (2018a), the values θ_r=0.045 and α=0.905 were adopted.

Based on the predicted scour depth performance that was integrated and studied by Sheppard et al. (2014), Neill (1964) formula (Eq. (3)), Shen et al. (1969) formula (Eq. (4)), Melville and Sutherland (1988) formula (Eq. (5)) and Froehlich (1991) formula (Eq. (6)) had a related accuracy on bridge pier scour depth estimation before 2000 year. Although some of the newer equations were proposed precisely to modify some elder ones, the parameters and coefficients may vary with different study locations or flow patterns. In addition, we refer to the study results by Lee et al. (2018b); some new and different kinds of empirical equations after 2000 years were selected to investigate their performance and feasibility. Therefore, the local scour depth evolution at the pier nose under unsteady flow is computed by a specific position proposed by Neill (1964) formula

(Eq. (3)), Shen et al. (1969) formula (Eq. (4)), Melville and Sutherland (1988) formula (Eq. (5)), Froehlich (1991) formula (Eq. (6)), Arneson et al. (2012) formula (Eq. (7)), and Qi et al. (2018) formula (Eq. (8)). The Eq. (8) was originally published by Sheppard et al. (2004) and later refined in their study by Sheppard et al. (2014). The Eq. (8) was refined and tested along with other published methods/equations using an extensive laboratory and field data set and found to be the most accurate of those tested. In this study, we proposed a local scour formula (Eq. (9)) by using the field-measured scour depth data to establish the regressed relationship as expressed in Eq. (9). The proposed equation is based on the parameters from Eqs. (17–22). Some equations are overly simplistic (e.g., Eq. 17), while most others contain too many uncertain or complex parameters (e.g., Eqs. 19–22). Therefore, we modified Eq. 18 to account for turbulence effects, presenting a new equation that better represents the flow mechanism and sediment transport performance under time-varying flow conditions, as described by WRA (2008) and Lee et al. (2018a, 2018b), in the study area. The adapted seven different empirical formulas are described as follows:

$$Y_S = 1.5D(Y_1/D)^{0.3} \tag{3}$$

$$Y_S = 2.5Y_1F_r^{2/3}(D/Y_1)^{0.6} \tag{4}$$

$$Y_s = Dk_sk_\alpha k_I k_y k_{\eta 4} k_\sigma \tag{5}$$

$$Y_S = 0.32\phi b^{0.62} Y_1^{0.47} F_r^{0.22} d_{50}^{-0.09} \tag{6}$$

$$Y_S = 2Y_1 k_s k_\alpha k_b k_w (D/Y_1)^{0.65} F_r^{0.43} \tag{7}$$

$$Y_s = b_* \left\{ \begin{array}{c} 2.5f_1f_2f_3, \quad 0.4 \le \overline{V}/V_c < 1 \\ f_1\left[2.2\left(\frac{\overline{V}/V_c-1}{V_p/V_c-1}\right)\right] + 2.5f_3\left(\frac{V_p/V_c-\overline{V}/V_c}{V_p/V_c-1}\right), \quad 1.0 \le \overline{V}/V_c < V_p/V \\ 2.2f_1, \quad \overline{V}/V_c \ge V_p/V_c \end{array} \right\}$$

$$f_1 = tanh\left[\left(Y_1/b_*\right)^{0.4}\right]$$

$$f_2 = 1 - 1.2\left[\ln\left(\overline{V}/V_c\right)\right]^2$$

$$f_3 = \frac{b_*/d_s}{0.4\left(\frac{b_*}{d_s}\right)^{1.2} + 10.6\left(\frac{b_*}{d_s}\right)^{-0.13}}$$

$$V_{p1} = 5V_c$$

$$V_{p2} = 0.6\sqrt{gY_1}$$

$$V_p = \left\{ \begin{array}{c} V_{p1} \ V_{p1} \ge V_{p2} \\ V_{p1} \ V_{p2} \ge V_{p2} \end{array} \right\} \tag{8}$$

$$Y_s = 0.2Y_1\left(Y_1/D\right)^{0.5} F_r^{0.25}\left(\bar{V}Y_1/\upsilon\right)^{0.12} \tag{9}$$

In which, Y_s = local scour depth; Y_1 = water depth of bridge upstream reach; F_r = Froude number of bridge upstream reach; ϕ = correction coefficient of bridge noise shape; ϕ = 1.3 for rectangular bridge noise; ϕ = 1.0 for rounded bridge noise; ϕ = 0.7 for triangle bridge noise; b = Pier width of transverse to the flow direction; D = Pier diameter; k_s = factor for pier shape; k_α = factors for flow angle of attack; k_b = factor for state of bed-sediment motion; k_w = factor for wide piers (for details, see Richardson and Davis 2001); k_I = factor of flow intensity; $k_{\eta 4}$ = factor of sediment size; k_σ = factor of sediment gradation(see details in Melville and Sutherland 1988); $\overline{V}$ is flow velocity; V_c = critical approach flow velocity for entrainment of bed sediment; b_* = effective diameter = projected width × shape factor Shape factor (= 1, circular; = 0.86 + 0.97($|\beta - \pi/4|)^4$,square); β = flow skew angle in radians and d_s = sediment size.

Results and discussion

Field monitoring measurement and scour process analysis

Since the installation of the bridge scour sensor system was completed in late 2015, the system has recorded scour and deposition measurements during two typhoon events:

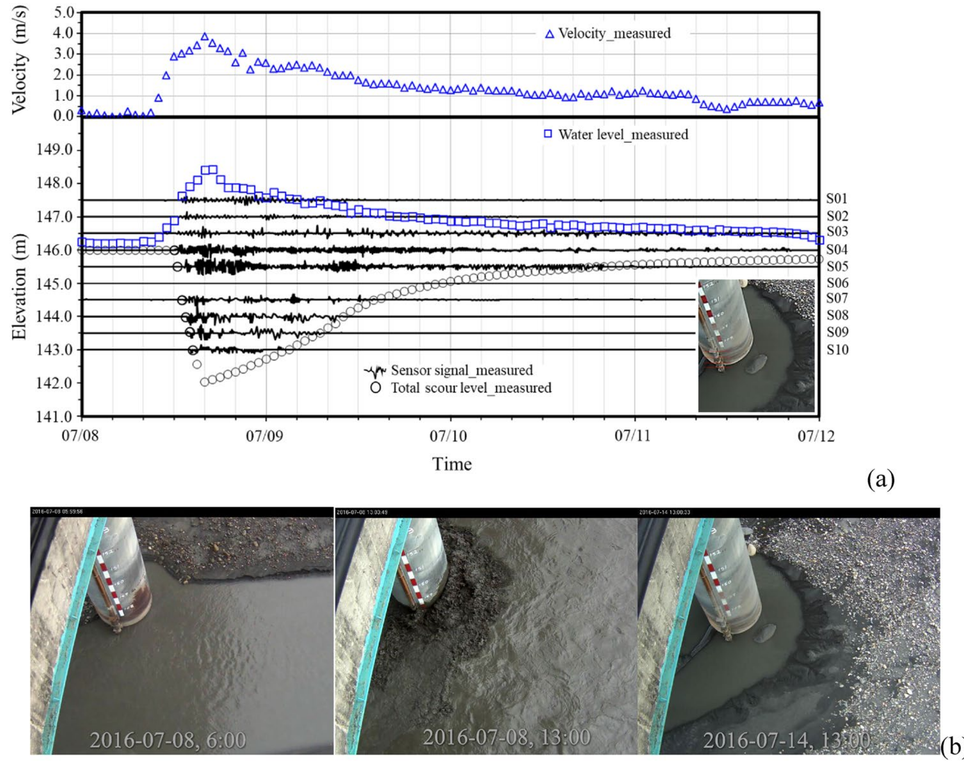

Fig. 4 Bridge scour/deposition history in Typhoon Nepartak (July 2016) **a** record data; **b** images

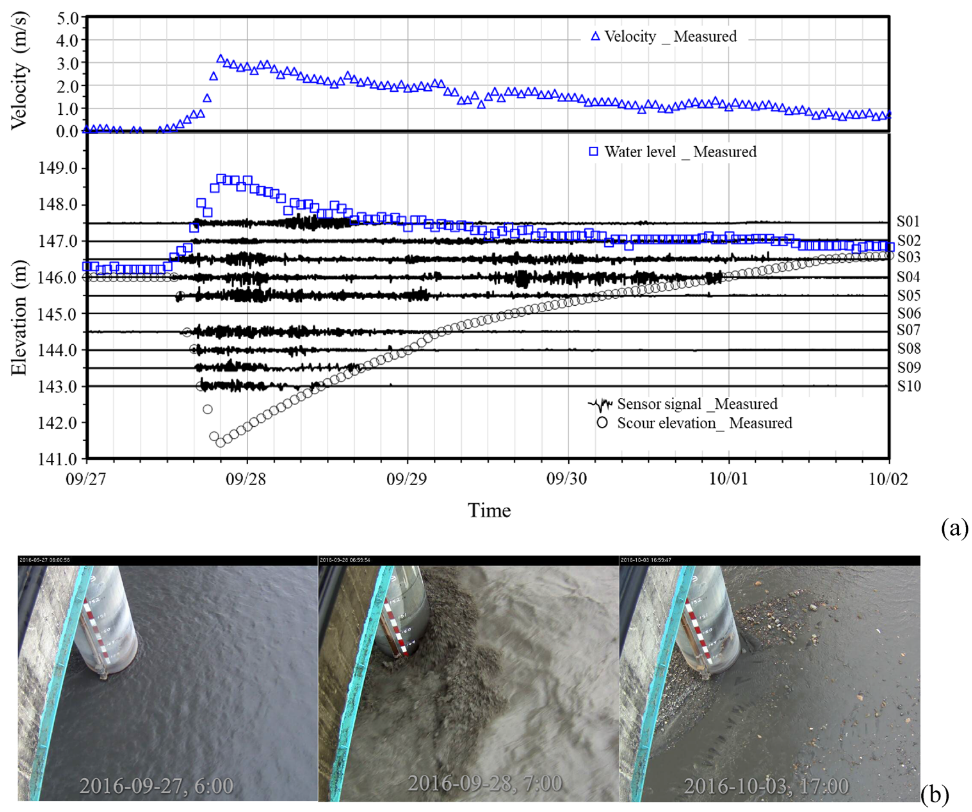

Fig. 5 Bridge scour/deposition history in Typhoon Megi (September 2016) **a** record data; **b** images

Typhoon Nepartak (July 8–13, 2016) (Fig. 4) and Typhoon Megi (September 27–October 1, 2016) (Fig. 5), both of which featured intense rainfall. Therefore, the data obtained from the scour sensors, water-level meter, and velocimeter during these two typhoon events were analyzed. In Fig. 4, the vibration readings from the ten scour sensor nodes are plotted against the time axis to represent the scour and deposition history during Typhoon Nepartak. The numbers in parentheses on the vertical axis indicate the sensor elevations relative to sea level. Unfortunately, sensor S06 at EL.145 m was not functional at the installation stage due to transmission failure, so its data are excluded from the figure. To assess the correlation between the vibration responses of the scour sensors and the changes in hydraulic parameters, the water level and velocity measurements are presented in the scour/deposition history diagram. The maximum water level and flow velocity are also denoted. Additionally, a solid thick line in the scour/deposition hydrographs highlights the original riverbed level. For traditional radar wave water level sensors, the radar echo signal will occasionally be confused due to flowing debris on the water surface, resulting in noise. At this time, a camera can be used to identify the water level from the painting water level of numbers, which can be used for calibrating the radar wave water level sensor. The camera can also record the size and depth of the scour hole at the bridge pier immediately after the water recedes.

In addition, the camera would also be used by bridge management personnel to watch the status of the bridge during a typhoon in real-time from the monitor in the office, including the painting water level indicated on the pier, without having to brave the risk of heavy typhoon winds and rain to conduct bridge inspections. The CCTV camera took field images to record real-time flow conditions and verify the accuracy of the water-level data collected by the radar water-level meter.

During flooding, the scouring monitoring system provided the impact of scour depth and its corresponding bridge safety. This structural pier foundation bearing capacity safety evaluation can be used to estimate and provide early warning of bridge erosion safety margin and carry out bridge closure contingency measures. From the deposition process, the bridge safety status would be evaluated from the deposition depth. Typically, the bridge piers in the deep water area were still in the flowing water area after the flooding, making it difficult to observe and evaluate the status of a foundation's safety. Similarly, through the monitoring system, the safety of a bridge during the back-silting depth could be assessed; as mentioned above, after we close the bridge, the traffic reopening would be based on the depth of sediment deposition safety evaluation.

According to the data recorded during Typhoon Nepartak, the flood-induced scour and deposition processes, as seen in Fig. 4, can be readily separated into two distinct stages: the scouring stage and the scour hole refilling stage (i.e., the deposition stage). When the typhoon-induced flood first impacted Pier P4 during the scouring stage, the rapidly rising floodwater submerged the sensor nodes (i.e., S01, S02, and S03) that were initially exposed to the air. Concurrently, the sensor nodes buried in sediments below the original riverbed level gradually emerged into the flow turbulence due to the erosion of riverbed materials around the pier. During the typhoon flood event, all the scour sensor nodes exhibited significant signal fluctuations in response to the flow turbulence. However, as time passed and the flow velocity and water level receded in the deposition stage, all the sensors ceased vibrating sequentially.

For example, the sensors S01 and S02 showed no signal fluctuation at 6:00 AM on July 9, when the water level dropped below EL.147 m. A trial-and-error process was conducted to calibrate a signal fluctuation threshold for each sensor. When the sensor reading exceeded its corresponding threshold, it was assumed to be exposed to flow turbulence and thus set in motion. The same threshold value was used to determine when the sensor settled. Based on the calibrated signal fluctuation threshold values for each sensor, the vibration onset and settlement of each scour sensor node are marked by circles, as shown in Fig. 4. The profile curves allow for the explicit definition of the pier scour and deposition stages, such as: a) the commencement of the pier scour stage is assumed to be the vibration onset of the topmost sensor node in the bed sediment; b) the instance at which the vibration of the deepest sensor (i.e., S10) diminishes is assumed to mark the completion of the scour stage and the beginning of the deposition stage; and c) the instant at which the last sensor settles due to local sediment deposition signifies the completion of the deposition stage.

However, the settlement of the scour sensors may be attributed to either the sensor emerging from the air or local sediment deposition. It is impractical to determine the cause of sensor settlement by merely relying on the readings of the scour sensors. Therefore, the water-level hydrograph is combined with the scour/deposition diagram, and the temporal length of the diagram is determined as the water level recedes to the riverbed. Given the water-level profile and a known reference elevation, sensor signals due to deposition can be readily distinguished. Specifically, when the vibration of scour sensors located below the reference elevation diminishes, these sensors are assumed to be buried by sediment deposits. Moreover, the settlement of the topmost scour sensor due to local deposition indicates the approximate final deposition height.

The feasibility of this approach for determining the final deposition height of the pier site channel was verified by the images recorded by the in-situ monitoring camera (Figs. 4 and 5). According to the post-flood images in both flood events (Figs. 4(b) and 5(b)), as the flood recedes, the riverbed resurfaces with two (i.e., S01–S04) and four (i.e., S01–S02) sensor nodes exposed. This observation is consistent with the tactically determined final deposition heights in the two typhoon events.

The results show that the innovative scour monitoring system using vibration-based MEMS sensors can provide the depth sequence of scouring and deposition around the bridge pier during typhoon-induced flood events. In addition, the adapted numerical model and formulas can appropriately simulate the variation of bridge pier scour depth. Therefore, the prediction module for bridge pier scour depth and field scour depth monitoring have been developed. In practice, based on rainfall predictions before flood events and flood forecasts in a river basin, an effective prediction system for the scour depth of bridge piers will be achieved in the future. Furthermore, MEMS technology can provide real-time bridge pier scour depth information, which could help assess bridge safety.

Total scour-depth evolution simulation in flood events

Based on the field survey data of hydrological conditions and bridge pier scour depth measurements in this study, the National Center for Research on Earthquake Engineering observed the scour depth at the bridge pier. An innovative scour monitoring system using vibration-based MEMS sensors was employed to provide data for numerical model calibration and verification. Additionally, historical flood events from 2013 to 2017 were collected. This study applies the SRH-1D numerical model to generate boundary conditions for the SRH-2D model and uses empirical formulas to estimate bridge pier scour depth. For the SRH-1D model, the adapted downstream water level is provided by the Central Weather Bureau, with the location set at Tai No.61 Western Coast Expressway. The Water Resources Agency provides the upstream hydrological conditions, and the tributary discharge is derived from field measurement data at Yanping and Longmen bridges. Figure 6 presents the simulated results for water level, velocity, and bed level changes. Compared to the measured data, both the SRH-1D and SRH-2D simulated results agree with the measured data.

Figure 7 shows the bridge pier scour depth based on field monitoring data at the Mingchu Bridge during Typhoon Soudelor (2015), Typhoon Dujuan (2015), Typhoon Nepartak (2016), and Typhoon Megi (2016). Hydrological patterns appear to correspond with the bridge pier's scour depth. The circle symbols represent the hydrographs of field scour depth monitoring data, including scour and deposition processes during flood events. Due to the monitoring elevation ranging from the riverbed to EL 143 m, the deepest monitoring depth is constrained at EL 143 m. Therefore, the monitoring sensors did not measure the deepest bridge scour depth during these flood events. Based on the field monitoring data, the total scour depth remained below EL 143 m during all flood events. Additionally, the vertical distance between sensors is 0.5 m, meaning the resolution of the measured scour and deposition intervals is also 0.5 m.

According to the monitoring data, the scour rate is higher than the deposition rate; however, the scour duration is shorter than the deposition duration. This indicates that the reaction time for the bridge safety management office is limited during the bridge scour process. Therefore, the reaction time would be constrained if the bridge safety warning system relies on field monitoring data alone. This highlights the importance of a reliable numerical model for predicting bridge pier scour depth. In general, Fig. 7 presents consistent simulation results of bridge pier scour depth across all flood events. Based on the simulation results, Arneson et al. (2012) overestimated the bridge pier scour depth and underestimated by Froehlich (1991). In contrast, the proposed formula aligns more closely with the monitoring data during both the scour and deposition processes.

Scoured bed level-discharge relationship for early warning

After model calibration and verification, the SRH-2D model can be used to determine the scour depth at each bridge pier under four major return-period floods, as shown in Figs. 8(a, b). The evolution of the maximum scour depth and the affected bridge piers correspond to the hydrological magnitude, aiding bridge safety management and establishing warning systems. During typhoon seasons in Taiwan, bridge managers typically base closure decisions on the river's discharge. This practice assumes that higher discharge leads to deeper scour holes, even though the precise relationship between flow depth and total scour depth at the piers is not generally known in advance. Using the SRH-2D model, this study provides a rational approach for evaluating the influence of discharge on the scoured bed level at the piers. Therefore, in this study, the bridge safety curve for the Mingchu Bridge has been established to assess bridge scour risk.

Based on the initial bed level, the calculated total scour depth at the bridge pier is assumed to occur on the approach bed. Numerical simulations were performed to evaluate the relationship between the scoured bed level and the corresponding discharge around the Mingchu Bridge in the Cho-Shui River, Taiwan. Four flood discharges were simulated, corresponding to 1.11-, 2-, 10-, and 100-year return-period floods. A statistical regression analysis was then conducted to develop the relationship between the scoured bed level and discharge within the mainstream cross-section along the Mingchu Bridge, typically at Piers P2-P7, as shown in Fig. 8(c). The scoured bed elevation (Z_b) is uniquely related to discharge (Q) and can be fitted to $Z_b = 163.70 \times Q^{-0.017}$

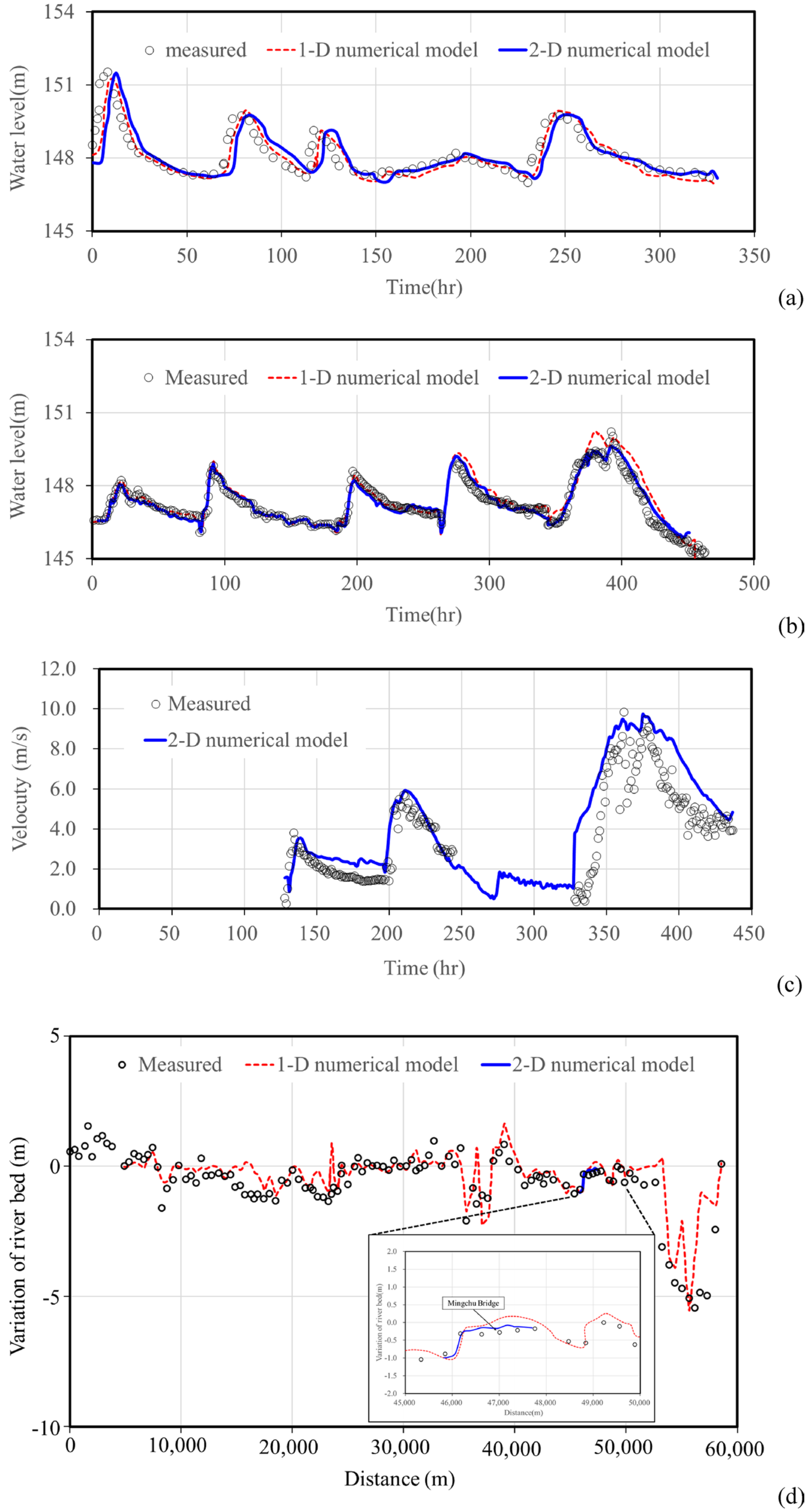

Fig. 6 Numerical simulation results **a** water elevation calibration of 2013 events; **b** water elevation verification between 2015 and 2017 events; **c** velocity verification between 2015 and 2017 events; **d** river bed verification

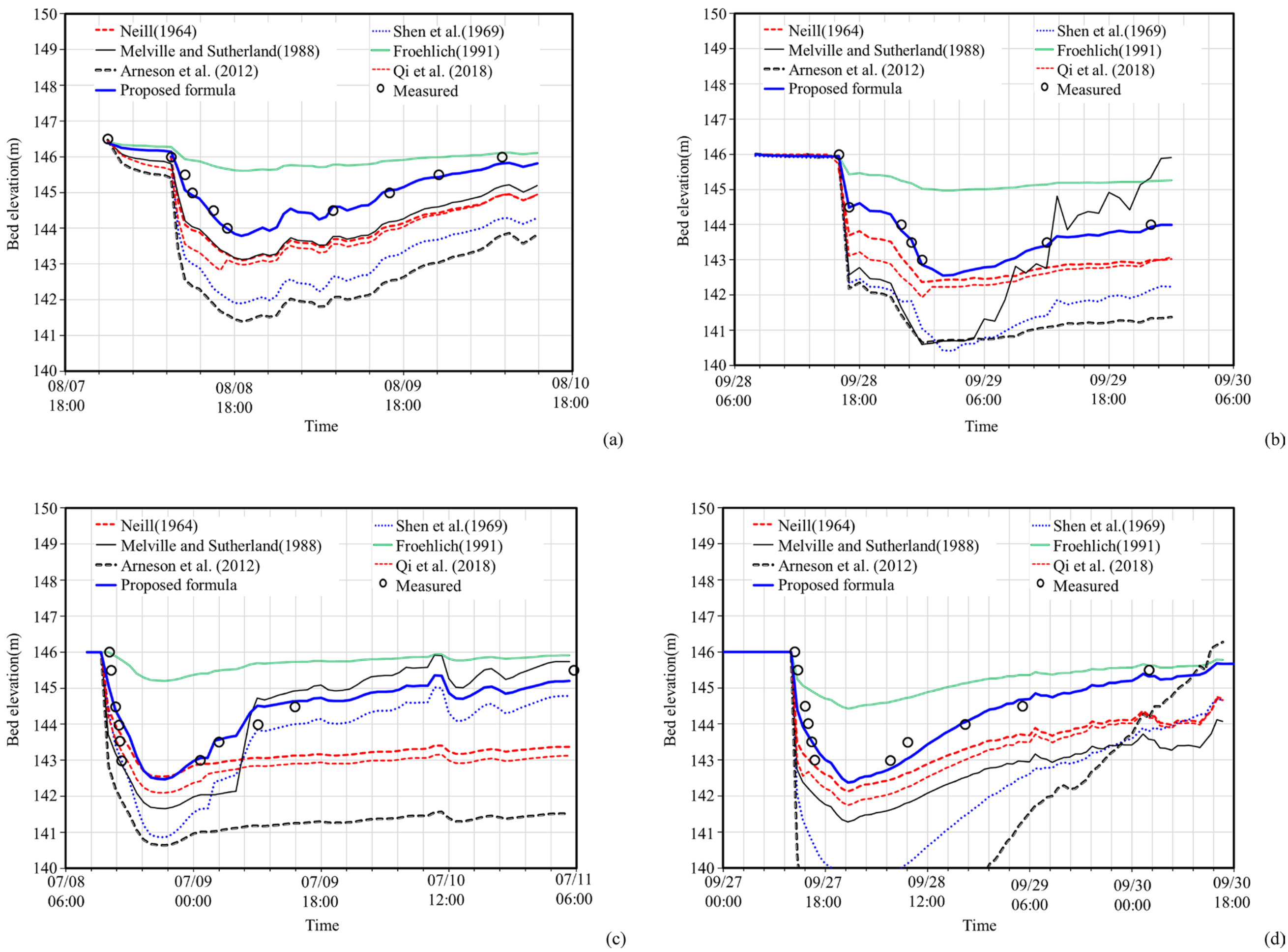

Fig. 7 Numerical simulation and estimation of bed elevation by SRH-2D during **a** Typhoon Soudelor; **b** Typhoon Dujuan; **c** Typhoon Nepartak; **d** Typhoon Megi

($R^2 = 0.989$), indicating that Z_b decreases with an increase in discharge. One can easily deduce the scour depth for a given flow discharge using this equation. To provide an assessment of scour risk for the scoured bed elevation with bridge pier foundation, three meaningful levels based on the pier foundation characteristics, the top and bottom levels of the pile cap (142.75 m and 139.75 m) and the level of the pile extension (129.75 m), are superimposed in Fig. 8(c). When the target bridge reaches its safety warning depth of bridge safety curve event due to erosion or scour, the flooding scour early warning monitoring system will automatically notify the bridge management agency to close the bridge through the alarm system. In addition, the traffic signals installed at the end of the bridge will continue to flash red lights to warn passing vehicles to avoid casualties and property losses caused by the bridge collapse. With these three reference levels referring to the bridge safety curve, based on the scoured bed level-discharge relationship in the study by Hong et al. (2016), four bridge warning stages are identified:

Safe: when bed elevation > EL. 142.75 m.

Low risk: when bed elevation < EL. 142.75 m and > EL. 139.75 m.

Moderate risk: when bed elevation < EL. 139.75 m and > EL. 129.75 m.

High risk: when bed elevation < EL. 129.75 m.

For instance, when the discharge exceeds $Q_{10} = 11{,}900$ m^3/s, Piers P5 and P4's scoured bed levels yield $Z_b = 139.55$ m and 138.89 m, respectively. The computed scoured bed level lies below the bottom of the cap, constituting a "moderate risk" condition. In summary, the proposed bridge safety curve (Fig. 8(c)) enables bridge managers to make rational decisions on bridge closures during flood events based solely on discharge values, as a determinate relationship between scoured bed level and discharge has been established.

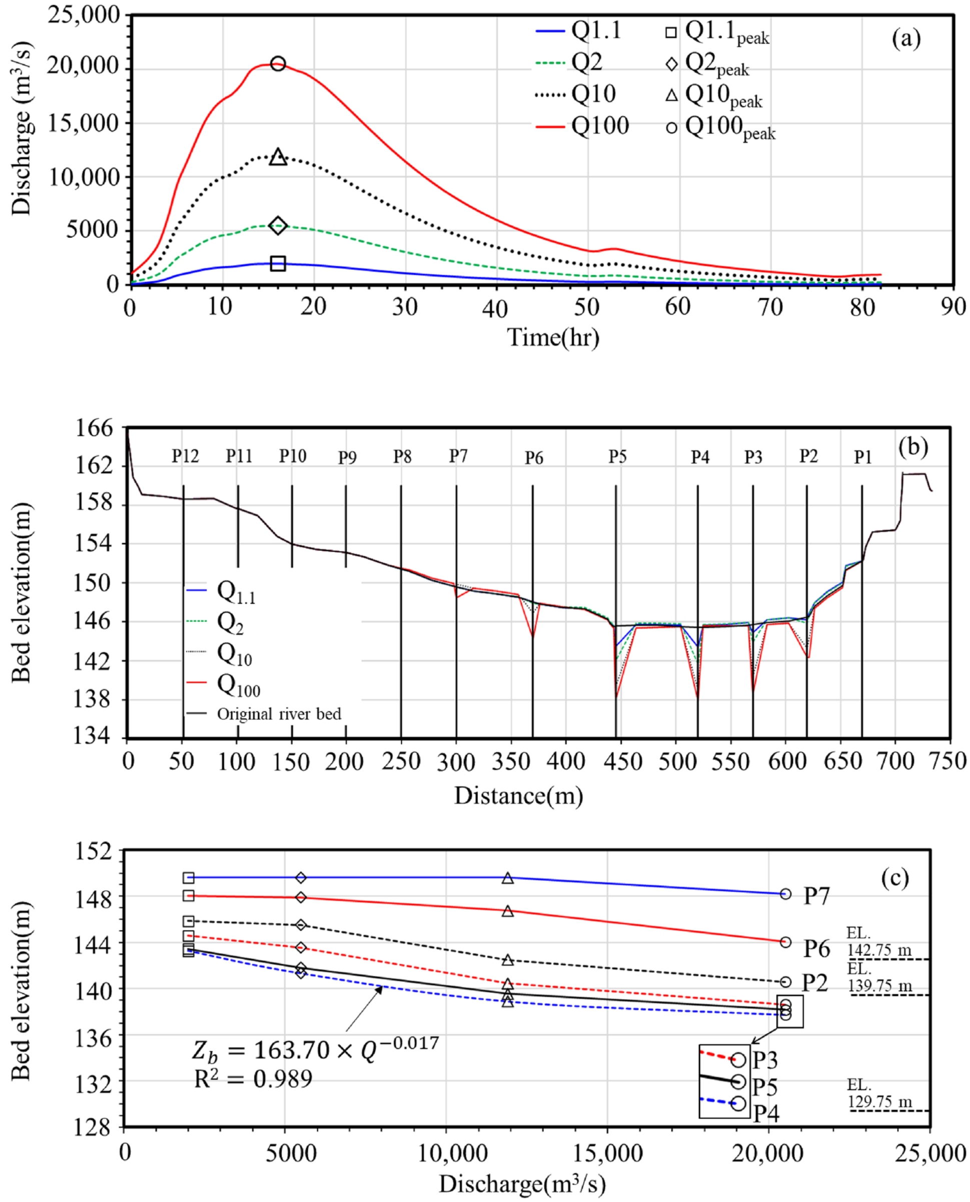

Fig. 8 Numerical simulation of **a** different return period flood **b** cross-section elevation **c** bridge safety curve

Conclusions

Scour-induced bridge collapse often occurs suddenly and unpredictably, posing severe threats to bridge traffic and lives. In response to this urgent need, reliable river-basin disaster monitoring and bridge-scour early-warning systems are developed in this study. The scour monitoring system consists of MEMS-based scour-arrayed sensors, along with water-level and flow-velocity measuring instruments on a traffic bridge for empirical field investigation.

For early warning purposes related to bridge safety and scour depth estimation, the SRH-1D and SRH-2D numerical models, combined with scour formulas, are applied to calculate water levels, flow velocities, riverbed changes, and bridge pier scour depths. Based on historical events in the study area, the calibration and verification of the SRH-1D and SRH-2D models for water levels, flow velocities, and topographic changes have been completed. The SRH-2D model is then used to estimate the bridge pier scour depth. A comparison of the simulated bridge pier scour depth with data from the monitoring system, which includes MEMS-based scour sensors, shows agreement between the simulated and observed scour and deposition processes. Both empirical and presented formulas are adapted to estimate bridge scour depth. The results indicate that the proposed local scour depth formula effectively estimates bridge pier scour depth.

Data analysis from two typhoon-induced flood events revealed that the depth-wise scour monitoring sensors effectively track scour development and deposition in real-time, responding to flow turbulence. This progress is evident in the profiles showing sensor vibration onset and settlement, clearly defining the scour and deposition processes. It was found that when the maximum scour depth is within the range of the sensors, the signal responses directly indicate the depth. However, the maximum depth cannot be precisely determined if the scour extends beyond the sensor range. Hence, a sensor matrix with a broader embedment range is preferable for accurate measurement.

Determining the final deposition height requires knowledge of the equilibrium water level or the re-emerging riverbed level, which can be estimated empirically or confirmed using field images from the monitoring camera. The signal responses and durations of the scour and deposition processes are closely linked to the duration of typhoon-induced rainfall and the intensity of the resulting flood (e.g., flow velocity and discharge volume). Thus, an in-situ monitoring camera is essential for real-time monitoring, as it provides valuable images that can help determine the post-flood equilibrium water level or riverbed level.

These analytical results confirm the effectiveness of the proposed scour monitoring system in assessing scour development and deposition at bridge sites. The study demonstrates how changes in flow velocity and water level influence the scour and deposition processes, providing reliable indications of maximum scour depth and final deposition height. Additionally, the study creates a valuable database for further hydraulic studies and bridge structural modeling, aiding in scour depth prediction and bridge safety assessments during flood events.

Adopting the numerical models to simulate riverbed scour and the influence of bridge construction on riverbed deformation, the scour depth can be estimated at each bridge pier in advance. The real-time scour monitoring system, combined with the numerical simulation module developed in this study, provides accurate information on scour and deposition processes at bridge piers. The risk-based methodology for scour analysis at bridge foundations is crucial for decision-makers to assess bridge damage risks and determine the appropriate timing for bridge closures. In addition, a risk-based approach to bridge scour prediction under various return-period floods is valuable for applications in bridge safety design.

The study also found that previous predictions by Arneson et al. (2012) tend to overestimate scour depth, while those by Froehlich (1991) tend to underestimate it, making the proposed formula more consistent with observed data. Finally, the proposed bridge safety curve establishes a clear relationship between scoured bed level and discharge and helps bridge managers make informed decisions about closures during typhoon seasons. By combining scour predictions with real-time monitoring data, bridge safety management is enhanced, improving both the timing of transportation restrictions and the opportunities for reopening.

Acknowledgements The authors acknowledge the Technical Service Center, United States Bureau of Reclamation, for the numerical software provided for this study. The writers also wish to thank the National Taiwan University and the National Center for Research on Earthquake Engineering for their support of human resources and techniques.

Author contributions Fong-Zuo Lee was responsible for simulation the hydraulic patterns and writing the article. Jihn-Sung Lai was responsible for inspecting the correctness of the methodology and approving the research contents. Yung-Bin Lin was responsible for the analysis and description of filed measurement data. Kuo-Chun Chang was responsible for ensuring the correctness of the framework.

Funding The presented study was supported by the National Science and Technology Council in Taiwan, and its Project numbers are NSTC 111–2221-E-005–092, NSTC 113–2625-M-002–018, and NSTC 113–2221-E-005–027.

Data availability No datasets were generated or analysed during the current study.

Declarations

Conflict of interest The authors declare that they have no conflict of interest to this work.

Ethical approval Not applicable.

Consent to participate Not applicable.

Consent to publish Not applicable.

References

Ahmed F, Rajaratnam N (1998) Flow around bridge piers. J Hydraul Eng 124(3):288–300. https://doi.org/10.1061/(ASCE)0733-9429(1998)124:3(288)

Andrews ED (2000) Bed material transport in the virgin river. Utah Water Resour Res 36:585–596

Arneson LA, Abt SR (1998) Vertical contraction scour at bridges with water flowing under pressure conditions. Transp Res Rec 1647(1):10–17

Arneson LA, Zevenbergen LW, Lagasse PF, Clopper PE (2012) Evaluating scour at bridges. Hydraulic Engineering Circular 18, Federal Highway Administration (HEC-18), 5th ed, Washington, DC.

Ballio F, Radice A (2003) A non-touch sensor for local scour measurements. J Hydraul Res 41(1):105–108. https://doi.org/10.1080/00221680309499934

Bao T, Swartz RA, Vitton S, Sun Y, Zhang C, Liu Z (2017) Critical insights for advanced bridge scour detection using the natural frequency. J Sound Vib 386:116–133. https://doi.org/10.1016/j.jsv.2016.06.039

Bento AM, Minh TQ, Ferradosa T, Sousa HS, Nguyen HX, Matos JC (2024) Study on the model to determine riverbed scour and the influence of bridge construction on riverbed deformation. Olympiad in Engineering Science. Springer Nature Switzerland, Cham, pp 69–76

Bento AM, Couto L, Pêgo JP, Viseu T (2018) Advanced characterization techniques of the scour hole around a bridge pier model. In: E3S Web of Conferences. https://www.e3s-conferences.org/articles/e3sconf/abs/2018/15/e3sconf_riverflow2018_05066/e3sconf_riverflow2018_05066.html

Bento AM, Gomes A, Viseu T, Couto L, Pêgo JP (2020) Risk-based methodology for scour analysis at bridge foundations. Engineering structures, 223, 111115. https://www.sciencedirect.com/science/article/pii/S0141029620313365

Bento AM, Viseu T, Pêgo JP, Couto L (2021) Experimental characterization of the flow field around oblong bridge piers. Fluids, 6(11), 370. https://www.mdpi.com/2311-5521/6/11/370

Bento AM, Gomes A, Viseu T, Couto L, Pêgo JP (2022) Assessment of scour risk in hydraulic infrastructures. A bridge case study. In: IABSE Symposium Prague 2022. https://doi.org/10.2749/prague.2022.1366

Bungton JM, Montgomery DR (1997) A systematic analysis of eight decades of incipient motion studies, with special reference to gravel-bedded rivers. Water Resour Res 33:1993–2029

Chang WY, Constantinescu G, Lien HC, Tsai WF, Lai JS, Loh CH (2013) Flow structure around bridge piers of varying geometrical complexity. J Hydraul Eng 139(8):812–826. https://doi.org/10.1061/(ASCE)HY.1943-7900.0000742

Chiew YM (2004) Local scour and riprap stability at bridge piers in a degrading channel. J Hydraul Eng 130(3):218–226. https://doi.org/10.1061/(ASCE)0733-9429(2004)130:3(218)

Clopper P, Lagasse PF, Zevenbergen LW (2014) Risk-Based Approach for Bridge Scour Prediction: Applications for Design. In: National Hydraulic Engineering Conference 2014 (Vol. 1, No. 2014). University of Iowa. https://onlinepubs.trb.org/onlinepubs/nchrp/docs/NCHRP24-34_FR.pdf

Deng L, Cai CS (2010) Bridge scour: prediction, modeling, monitoring, and countermeasures. Pract Period Struct des Constr 15(2):125–134. https://doi.org/10.1061/(ASCE)SC.1943-5576.0000041

Ding Y, Yan T, Yao Q, Dong X, Wang X (2016) A new type of temperature-based sensor for monitoring of bridge scour. Measurement 78:245–252. https://doi.org/10.1016/j.measurement.2015.10.009

Duffy K, Gavin K, Korff M, de Lange D, Roubos A (2024) Influence of installation method on the axial capacity of piles in very dense sand. J Geotech Geoenviron Eng 150(6):04024043

Federico F, Silvagni G, Volpi F (2003) Scour vulnerability of river bridge piers. J Geotech Geoenviron Eng 129(10):890–899. https://doi.org/10.1061/(ASCE)1090-0241(2003)129:10(890)

Fisher M, Atamturktur S, Khan AA (2013a) A novel vibration-based monitoring technique for bridge pier and abutment scour. Struct Health Monit 12(2):114–125. https://doi.org/10.1177/1475921713476332

Fisher M, Chowdhury MN, Khan AA, Atamturktur S (2013b) An evaluation of scour measurement devices. Flow Meas Instrum 33:55–67. https://doi.org/10.1016/j.flowmeasinst.2013.05.001

Froehlich DC (1991). Analysis of onsite measurements of scour at piers. In: Proc., ASCE, National Hydraulic Engineering Conference, Colorado Springs, CO.

Gao Q, Yu XB (2015) Design and evaluation of a high sensitivity spiral TDR scour sensor. Smart Mater Struct 24(8):085005

Greimann BP, Vandeberg M (2008) Predicting rock scour. Technical Rep. SRH-2008–01, Bureau of Reclamation, US Dept. of the Interior, Denver.

Greimann BP (2011) SRH-1D 2.8 User's Manual. Sedimentation and River Hydraulics–One Dimension, Version, 2.8. U.S. Dept. of the Interior, Bureau of Reclamation, Technical Service Center, Sedimentation and River Hydraulics Group.

Guo WD, Hong JH, Chen CH, Su CC, Lai JS (2017) A simplified simulation method for flood-induced bend scour—a case study near the Shuideliaw embankment on the Cho-Shui River. Water 9(5):324. https://doi.org/10.3390/w9050324

Guo WD., Hong JH., Lee FZ, Lai JS (2014) Bridge scour prediction using 2D hydraulic model with empirical equations—a case study of Shuangyuan Bridge piers on the Kao-Ping River. In: Proceedings of the 6th World Conference on Structural Control and Monitoring, Barcelona, Spain 15–17.

Gupta LK, Pandey M, Raj PA, Pu JH (2023) Scour reduction around bridge pier using the airfoil-shaped collar. Hydrology 10(4):77. https://doi.org/10.3390/hydrology10040077

Highway Bureau (2020) The application of high-tech monitoring equipment to diagnose bridge health indicators and monitoring plans, MOTC.

Hogan SA (2018) Advancements in bridge scour assessment with 2D Hydraulic modeling using SRH-2D/SMS. In: book: Scour and Erosion IX, 283–287

Hong JH, Guo WD, Chiew YM, Chen CH (2016) A new practical method to simulate flood-induced bridge pier scour—a case study of Mingchu bridge piers on the Cho-Shui River. Water 8(6):238. https://doi.org/10.3390/w8060238

Hong JH, Guo WD, Wang HW, Lee FZ, Lin YB (2014) Field measurement and simulation of riverbed and bridge scour in Cho-Shui River in Taiwan. In: Sixth World Conference on Structural Control and Monitoring, 6WCSCM, Barcelona, Spain.

Invernizzi S, Lacidogna G, Manuello A, Carpinteri A (2011) AE monitoring and numerical simulation of a two-span model masonry arch bridge subjected to pier scour. Strain 47:158–169. https://doi.org/10.1111/j.1475-1305.2010.00752.x

Komar (1989) Flow competence of the hydraulic parameters of floods. In: Beven K, Carling P (eds) Floods hydrological, sedimentological and geomorphological implications. John Wiley and Sons, Chichester, pp 107–134

Kong X, Ho SCM, Song G, Cai CS (2017) Scour monitoring system using fiber Bragg grating sensors and water-swellable polymers. J Bridg Eng 22(7):04017029. https://doi.org/10.1061/(ASCE)BE.1943-5592.0001062

Lai YG (2009) Watershed runoff and erosion modeling with a hybrid mesh model. J Hydrol Eng 14(1):15–26. https://doi.org/10.1061/(ASCE)1084-0699(2009)14:1(15)

Lai YG (2010) Two-dimensional depth-averaged flow modeling with an unstructured hybrid mesh. J Hydraul Eng 136(1):12–23. https://doi.org/10.1061/(ASCE)HY.1943-7900.0000134

Lai YG (2017) Modeling stream bank erosion: practical stream results and future needs. Water 9(12):950. https://doi.org/10.3390/w9120950

Lai YG (2020) A two-dimensional depth-averaged sediment transport mobile-bed model with polygonal meshes. Water 12(4):1032. https://doi.org/10.3390/w12041032

Lee FZ, Lai JS, Lin YB, Chang KC, Liu XQ, Huang CC (2018a) Prediction of bridge pier scour depth and field scour depth monitoring. In: Ninth International Conference on Fluvial Hydraulics, Lyon-Villeurbanne, France 40: 03007

Lee FZ, Lai JS, Lin YB, Chang KC, Huang CC, Lee BH, Gu MH, Liu XQ (2018b) Numerical Simulation for the Estimation of Scour Depth at Bridge Pier——A Case Study of MinChu Bridge in the Zhuoshui River. Taiwan Water Conservancy, Vol. 66, No. 3.

Lin YB, Chen JC, Chang KC, Chern JC, Lai JS (2005) Real-time monitoring of local scour by using fiber Bragg grating sensors. Smart Mater Struct 14(4):664–670. https://doi.org/10.1088/0964-1726/14/4/025

Lin YB, Lai JS, Chang KC, Li LS (2006) Flood scour monitoring system using fiber Bragg grating sensors. Smart Mater Struct 15(6):1950–1959. https://doi.org/10.1088/0964-1726/15/6/051

Lin YB, Lai JS, Chang KC, Chang WY, Lee FZ, Tan YC (2010) Using MEMS sensors in the bridge scour monitoring system. J Chin Inst Eng 33(1):25–35. https://doi.org/10.1080/02533839.2010.9671593

Lin CP, Wang K, Chung CC, Weng YW (2017) New types of time domain reflectometry sensing waveguides for bridge scour monitoring. Smart Mater Struct 26(7):075014. https://doi.org/10.1088/1361-665X/aa71f9

Lin YB, Lee FZ, Chang KC, Lai JS, Lo SW, Wu JH, Lin TK (2021) The artificial intelligence of things sensing system of real-time bridge scour monitoring for early warning during floods. Sensors 21(14):4942. https://doi.org/10.3390/s21144942

Link O, García M, Pizarro A, Alcayaga H, Palma S (2020) Local scour and sediment deposition at bridge piers during floods. J Hydraul Eng 146(3):04020003. https://doi.org/10.1061/(ASCE)HY.1943-7900.0001696

Lu JY, Hong JH, Su CC, Wang CY, Lai JS (2008) Field measurements and simulation of bridge scour depth variations during floods. J Hydraul Eng 134(6):810–821. https://doi.org/10.1061/(ASCE)0733-9429(2008)134:6(810)

Melville BW, Coleman SE (2000) Bridge scour. Water Resources Publications, Highlands Ranch

Melville BW, Sutherland AJ (1988) Design method for local scour at bridge piers. J Hydraul Eng 114(10):1210–1226. https://doi.org/10.1061/(ASCE)0733-9429(1988)114:10(1210)

Melville B, Van Ballegooy S, Coleman S, Barkdoll B (2006) Scour countermeasures for wing-wall abutments. J Hydraul Eng 132(6):563–574. https://doi.org/10.1061/(ASCE)0733-9429(2006)132:6(563)

Miyata S, Fujita M (2018) Laboratory based continuous bedload monitoring in a model retention basin: application of time domain reflectometry. Earth Surf Proc Land 43(9):2022–2030. https://doi.org/10.1002/esp.4358

Neill CR (1964) River bed Scour, a review for bridge engineers. Contract No. 281, Res. Council of Alberta, Calgary, Alberta, Canada. https://trid.trb.org/View/97055

Parker G (1990) Surface-based bedload transport relation for gravel rivers. J Hydraul Res 28(4):417–436. https://doi.org/10.1080/00221689009499058

Prendergast LJ, Gavin K (2014) A review of bridge scour monitoring techniques. Journal of Rock Mechanics and Geotechnical Engineering 6(2):138–149. https://doi.org/10.1016/j.jrmge.2014.01.007

Proske D (2018) Bridge collapse frequencies versus failure probabilities, vol 8. Springer, Cham

Qi M, Li J, Chen Q (2018) Applicability analysis of pier-scour equations in the field: error analysis by rationalizing measurement data. J Hydraul Eng 144(8):04018050. https://doi.org/10.1061/(ASCE)HY.1943-7900.0001497

Rashidyan S, Ng TT, Maji A (2017) Estimating the depth of concrete pier wall bridge foundations using nondestructive sonic echo. J Nondestr Eval 36:1–17

Richardson EV, Davis SR (2001) Evaluating scour at bridges. Hydraulic engineering circular no. FHWA NHI 01–001 (HEC-18), 4th edn. Federal Highway Administration, Washington, DC

Sakhaee F (2020) REMOVED: steady and unsteady flow simulation with SRH-2D. J Ocean Eng Sci 5(4):297–309. https://doi.org/10.1016/j.joes.2020.01.002

Shen HW, Schneider VR, Karaki S (1969) Local scour around bridge piers. J Hydraul Div 95(6):1919–1940. https://doi.org/10.1080/00221688709499285

Vahdati VJ, Ahmadi A, Abedini A, Heidarpour M (2024) Efficacy of the combined use of bed sill and sacrificial piles to control local scour around circular bridge piers. Shock Vibration 2024(1):5527946. https://doi.org/10.1155/2024/5527946

Wang CY, Wang HL, Ho CC (2012) A piezoelectric film type scour monitoring system for bridge pier. Adv Struct Eng 15(6):897–905. https://doi.org/10.1260/1369-4332.15.6.897

Wang C, Yu X, Liang F (2017) A review of bridge scour: mechanism, estimation, monitoring and countermeasures. Nat Hazards 87:1881–1906. https://doi.org/10.1007/s11069-017-2842-2

Wang G, Liang D, Yan J (2018) A vibration-based method for the measurement of subgrade soil scaling factor. Photonic Sens 8:375–383

Water Resources Agency (WRA) (2008) Rock Erosion Modeling on Selected Alluvial Rivers in Taiwan. Bureau of Reclamation, US Dept. of the Interior, Denver.

Wilcox PR, Crowe JC (2003) Surface-based transport model for mixed-size sediment. J Hydraul Eng 2003(129):120–128

Wu WH, Prendergast LJ, Gavin K (2018) An iterative method to infer distributed mass and stiffness profiles for use in reference dynamic beam-Winkler models of foundation piles from frequency response functions. J Sound Vib 431:1–19. https://doi.org/10.1016/j.jsv.2018.05.049

Yang Y, Melville BW, Macky GH, Shamseldin AY (2020) Temporal evolution of clear-water local scour at aligned and skewed complex bridge piers. J Hydraul Eng 146(4):04020026. https://doi.org/10.1061/(ASCE)HY.1943-7900.0001732

Yang Y, de Lange DA, Wang H, Askarinejad A (2024) Multi-scale calibration of a line-style sand pluviator. Geomech Eng 37(5):431–441

Ye XW, Su YH, Xi PS (2018) Statistical analysis of stress signals from bridge monitoring by FBG system. Sensors 18(2):491. https://doi.org/10.3390/s18020491

Yu X, Zhang B, Tao J, Yu X (2013) A new time-domain reflectometry bridge scour sensor. Struct Health Monit 12(2):99–113. https://doi.org/10.1177/1475921713476331

Zarafshan A, Iranmanesh A, Ansari F (2012) Vibration-based method and sensor for monitoring of bridge scour. J Bridg Eng 17(6):829–838. https://doi.org/10.1061/(ASCE)BE.1943-5592.0000362

Zheng W, Yu W (2015) Probabilistic approach to assessing scoured bridge performance and associated uncertainties based on vibration measurements. J Bridg Eng 20(6):04014089. https://doi.org/10.1061/(ASCE)BE.1943-5592.0000683

Zhou Z, Huang M, Huang L, Ou J, Chen G (2011) An optical fiber Bragg grating sensing system for scour monitoring. Adv Struct Eng 14(1):67–78. https://doi.org/10.1260/1369-4332.14.1.67